Biogeosciences Discuss., 9, 12309–12341, 2012
www.biogeosciences-discuss.net/9/12309/2012/
doi:10.5194/bgd-9-12309-2012
© Author(s) 2012. CC Attribution 3.0 License.

Biogeosciences Discussions

This discussion paper is/has been under review for the journal Biogeosciences (BG).
Please refer to the corresponding final paper in BG if available.

Arctic microbial community dynamics influenced by elevated CO_2 levels

C. P. D. Brussaard[1], A. A. M. Noordeloos[1], H. Witte[1], M. C. J. Collenteur[1], K. Schulz[2], A. Ludwig[2], and U. Riebesell[2]

[1]Department of Biological Oceanography, NIOZ – Royal Netherlands Institute for Sea Research, P.O. Box 59, 1790 AB Den Burg, Texel, The Netherlands
[2]Helmholtz Centre for Ocean Research (GEOMAR), Kiel, Germany

Received: 10 August 2012 – Accepted: 10 August 2012 – Published: 12 September 2012

Correspondence to: C. P. D. Brussaard (corina.brussaard@nioz.nl)

Published by Copernicus Publications on behalf of the European Geosciences Union.

Abstract

The Arctic Ocean ecosystem is particular vulnerable for ocean acidification (OA) related alterations due to the relatively high CO_2 solubility and low carbonate saturation states of its cold surface waters. Thus far, however, there is only little known about the consequences of OA on the base of the food web. In a mesocosm CO_2-enrichment experiment (overall CO_2 levels ranged from ~180 to 1100 µatm) in the Kongsfjord off Svalbard, we studied the consequences of OA on a natural pelagic microbial community. The most prominent finding of our study is the profound effect of OA on the composition and growth of the Arctic phytoplankton community, i.e. the picoeukaryotic photoautotrophs and to a lesser extent the nanophytoplankton prospered. A shift towards the smallest phytoplankton as a result of OA will have direct consequences for the structure and functioning of the pelagic food web and thus for the biogeochemical cycles. Furthermore, the dominant pico- and nanophytoplankton groups were found prone to viral lysis, thereby shunting the carbon accumulation in living organisms into the dissolved pools of organic carbon and subsequently affecting the efficiency of the biological pump in these Arctic waters.

1 Introduction

The increase of pCO_2 in the surface ocean (ocean acidification, OA) profoundly affects the seawater carbonate system through well-known chemical reactions, lowering the pH, increasing the concentration of bicarbonate ions, decreasing the availability of carbonate ions and lowering the saturation state of the major shell-forming carbonate minerals. Whereas surface water pH values were still 8.2 just prior to the industrial era, they are 8.11 at present and anticipated to reach 7.8 in the year 2100 (The Royal Society, 2005). This corresponds to CO_2 levels of 380 µatm at present to a projected high of at least 750 µatm by the end of this century.

BGD
9, 12309–12341, 2012

Changes in carbonate chemistry can be expected to directly affect phytoplankton photosynthesis and subsequently growth because of their dependence on CO_2 supply. Not all algal groups will be equally affected as certain groups (most notably diatoms) have developed CO_2-concentrating mechanisms (CCMs). However, algal species differ in CCM efficiency (Rost et al., 2008). Non-calcifying phytoplankton show, as expected, a range of responses, varying from no effect on growth to stimulating or adverse effect on growth or primary production (Riebesell and Tortell, 2011). Only few studies have reported on phytoplankton composition changes (Tortell et al., 2002; Engel et al., 2008; Meakin and Wyman, 2011; Feng et al., 2009). The ecological consequences of OA on natural phytoplankton dynamics are still understudied.

Furthermore, a major gap in our understanding of concerns the transfer of responses from the organism to the community and ecosystem levels. Rose and coworkers (2009) recently showed that such changes in trophic dynamics can be substantial. As a result, predicting the impact of ocean acidification on marine ecosystem dynamics, and consequently biogeochemical cycling, is presently still limited. As pointed out by The Royal Society (2005), marine ecosystems are likely to become less robust as a result of ocean acidification and will be more vulnerable to other environmental changes (e.g. temperature increase, light availability, nutrient limitation). Potential restructuring of the phytoplankton community (classes, species and cell size; Falkowski et al., 1998; Boyd and Doney, 2002) as a result of ocean acidification will have direct consequences for grazer communities and organic carbon flow. It may also influence the dominance of grazing over other loss processes such as viral lysis and consequently the cycling of energy and biogeochemical relevant elements, the ratio of production and respiration of the ocean and the efficiency of the biological pump (Brussaard et al., 1996, 2008; Ruardij et al., 2005; Suttle, 2007). Phytoplankton that are consumed by grazers are channeled to higher trophic levels, whereas viral lysis directly forces the food web towards a more regenerative pathway (Brussaard et al., 2005; Suttle, 2007).

OA and other global climate change related impacts are most striking in both polar regions, where temperatures and acidities are changing at more than twice the global

BGD
9, 12309–12341, 2012

average (Hoegh-Guldberg and Bruno, 2010). The cold Arctic surface waters allow relatively high CO_2 solubility, making this area particularly vulnerable to OA. The present study is part of a collaborative mesocosm CO_2-enrichment experiment performed in Kongsfjorden off Svalbard, summer 2010, within the framework of the European Project on Ocean Acidification (EPOCA). We present here the microbial community dynamics under the influence of elevated pCO_2 levels and discuss the consequences for the functioning of the pelagic food web.

2 Material and methods

2.1 Study site and experimental set-up

The study was conducted in Kongsfjorden (78°56.2′ N and 11°53.6′ E), near Ny Ålesund, Svalbard, between 31 May and 7 July 2010 (Day $t-7$ to $t30$). Nine large mesocosms of approximately 50 m^3 (15 m below sea level) were moored in the fjord in sets of 3. The mesocosms were filled with fjord water (inorganic nutrient concentrations <0.1, 0.09, 0.2 and 0.7 µM for nitrate, phosphate, silicate and ammonium, respectively), screened through a 3 mm mesh to eliminate larger organisms on the 1 June ($t-6$). The mesocosms were open to the atmosphere but covered with transparent hoods to minimize input of rain and bird droppings. Two of the mesocosms received no CO_2 addition, representing the present day carbonate chemistry of the fjord ($\sim$185 µatm at the start of the experiment). The other 7 mesocosms were enriched with CO_2 over a period of several days ($t-1$ to $t4$) in varying amounts, resulting in a range of initial pCO_2 levels from $\sim$270 to $\sim$1420 µatm (corresponding to pH_T values of 8.18 to 7.51). Two weeks into the experiment ($t13$) inorganic nutrients were added to the originally nutrient-poor water in order to stimulate primary production (5 µM nitrate, 0.3 µM phosphate and 2.5 µM silicate for all mesocosms). The experimental set-up, carbon chemistry dynamics and nutrient concentrations throughout the experiment are described in detail by Riebesell et al. (2012); Bellerby et al. (2012) and Schulz et

BGD
9, 12309–12341, 2012

al. (2012). The one month experiment showed 4 phases: phase 0 represents the period from closing of the mesocosms to the end of the CO_2 manipulations ($t-7$ to $t3$), phase 1 corresponds to the period after CO_2 manipulation until the addition of inorganic nutrients ($t4$ to $t13$), phase 2 stands for the period after nutrient addition and until the second chlorophyll minimum ($t13$ to $t21$; Schulz et al., 2012), and phase 3 includes the final period until the end of the experiment ($t22$ to $t30$). Throughout this study the data are presented using 3 colors (blue, grey and red), representing low, intermediate and high pCO_2 additions. The low pCO_2 addition group contains mesocosms 3, 7 and 2; the intermediated group consists of mesocosms 4, 8 and 1; and the high pCO_2 addition group is made up of mesocosms 6, 5 and 9.

Collective sampling was performed daily in the morning using an integrated water sample (0–12 m). From this water subsamples were obtained for counting phytoplankton, HP and viruses. Besides, we sampled 2–3 times per week for the microzooplankton grazing incubations using a gentle vacuum-driven pump system. Samples were protected against daylight by black plastic bags. In the laboratory the samples were maintained (counting) and processed (grazing assay) at in situ temperature and dimmed light. The abundances of phytoplankton were determined on fresh samples. HP and viruses were fixed for 30 min at 7 °C with glutaraldehyde (25 %, EM-grade) at a final concentration of 0.5 % before snap freezing in liquid nitrogen and storage at −80 °C until analysis.

2.2 Microbial abundances

The microbes were enumerated using a bench-top Becton Dickinson FACSCalibur flow cytometer (FCM) equipped with a 488 nm argon laser. The photoautotrophic cells (< 20 µm) were counted fresh and discriminated by their pigment autofluorescence (Marie et al., 1999). Only eukaryotic photosynthetic organisms were detected. Based on their autofluorescence and side scatter signal, the phytoplankton community could be divided into 6 clusters: Picophytoplankton I and II, and Nanophytoplankton I to IV. Nanophytoplankton III and IV displayed higher side scatter signals than other clusters

BGD
9, 12309–12341, 2012

similar in size. Average cell size of the different clusters was determined by serial gravity filtration of a very small volume of sample (< 10 ml) through different polycarbonate 47 mm diameter filters (10, 8, 5, 3, 2, 1, 0.8, 0.4 µm) according to Veldhuis and Kraay (2004). Cell sizes of the different clusters ranged between 0.8–2, 2–3, 3–8, 8–10, 5–8 and 3–5 µm diameter for Picophytoplankton I, II, Nanoeukayotes I, II, III, and IV respectively. Assuming the cells to be spherical and containing 0.2 pg C μm^{-3} (Cuvelier, 2010), cellular carbon was calculated based on the average cell diameters (1.3, 3, 5, 10, 7 and 4 µm respectively). Estimated cellular carbon contents were 0.18, 2.8, 13.1, 104, 35.8 and 6.7 pg C $cell^{-1}$ for the 6 phytoplankton clusters respectively (Veldhuis and Kraay, 2004). Net growth and loss rates of phytoplankton were derived from exponential regression analysis of the cell abundances.

The abundances of heterotrophic prokaryotes (HP) and viruses were determined from fixed, frozen samples according to Marie et al. (1999) and Brussaard (2004), respectively. In short, thawed samples were diluted with Tris-EDTA buffer (10 mM Tris-HCl and 1 mM EDTA, pH 8) and stained with the green fluorescent nucleic acid-specific dye SYBR-Green I (Molecular Probes, Invitrogen Inc.) at a final concentration of 1×10^{-4} (HP) or 0.5×10^{-4} (viruses) of the commercial stock, in the dark at room temperature for 15 and 10 min, respectively. HP and viruses were discriminated in bivariate scatter plots of green fluorescence versus side scatter. Final counts were corrected for a blank consisting of TE-buffer and SYBR-Green I prepared and analysed in an identical manner to the samples. Two HP clusters (HDNA – high DNA fluorescent and LDNA – low DNA fluorescent) and 5 viral groups (V1–V5) were distinguished.

2.3 Microzooplankton grazing

Microzooplankton grazing of phytoplankton was determined using the dilution method of Landry and Hassett (1982). In short, whole seawater samples were sieved through a 200 µm mesh to remove mesozooplankton after which the sample was combined with 0.45 µm filtered seawater (0.45 µm Sartopore capsule filter, containing a 0.8 µm pre-filter) over a dilution series of 20, 40, 70 and 100 % to create a gradient in

BGD
9, 12309–12341, 2012

microzooplankton grazing pressure. All treatments were set up in triplicate in clear 1.2 l polycarbonate bottles. The bottles were incubated at in situ temperature and natural light. Subsamples were taken at 0 and 24 h and phytoplankton abundance was enumerated immediately by FCM. Phytoplankton growth rates were plotted against the level of dilution and model 1 regression analysis was performed to obtain the actual microzooplankton grazing rate (slope) and apparent phytoplankton growth rate in the absence of grazing (intercept y-axis). All seawater handling was performed at in situ temperature and under dim light conditions using Nitrile gloves. For logistical reasons we could only handle two dilution assays at a time. We choose to sample mesocosm 3, representing present time pCO_2 level, as reference for mesocosm 8 (intermediate pCO_2 levels) and mesocosm 5 (high pCO_2 levels) which each were sampled alternating. Microzooplankton grazing on nanophytoplankton II–IV failed due to the low whole water abundances ($< 200\,ml^{-1}$).

3 Results

3.1 Phytoplankton abundances and net growth

The abundance of each phytoplankton cluster is presented in Fig. 1. Total phytoplankton abundance was strongly dominated by the picoeukaryotic algal cluster I (Fig. 1a), generally making up more than 90 % of the total count except for $t1$–11 when their share declined down to 60 % of total due to a bloom of nanophytoplankton (Fig. 1b). Picophytoplankton I showed a steady increase until $t18$ after which the bloom declined sharply (Fig. 1a). The net growth rates during phase 1, derived from the standing stock and calculated using the natural logarithm, were on average 0.14 ± 0.03, 0.15 ± 0.03 and 0.17 ± 0.02 for the low, intermediate and high pCO_2 mesocosms, respectively. During phase 2, after inorganic nutrient addition, the net growth rates of the Picophytoplankton I were slightly higher, ranging from 0.13 to $0.24\,d^{-1}$. The high pCO_2 mesocosms showed the highest average net growth rate (on average $0.23 \pm 0.01\,d^{-1}$). Highest

BGD
9, 12309–12341, 2012

net peak abundances, 1.1–1.5 × 10^5 cells ml^{-1}, were also recorded for the high pCO_2 mesocosms 5, 6, and 9. Picophytoplankton II increased until $t6$ at a net growth rate between 0.30 and 0.38 d^{-1} (Fig. 1b). The highest abundance of 1.5–1.7 × 10^3 cells ml^{-1} was observed for the intermediate and low pCO_2 mesocosms.

Nanophytoplankton I increased steeply from the start of the experiment, growing at net growth rates between 0.51 and 0.55 d^{-1} (with the exception of mesocosm 4 showing a growth rate of 0.42 d^{-1}), and peaked at $t4$–6 with maximum abundances between 1.6 and 1.8 × 10^3 cells ml^{-1} (Fig. 1c). A second increase was found during the last week of the experiment with highest abundances typically in the higher pCO_2 meososms. Nanophytoplankton II were present in low numbers (generally below 150 cells ml^{-1}) and could no longer be detected in either the mesocosms or the natural fjord water from $t10$ onwards (Fig. 1d). Around the same time ($t6$) a new phytoplankton population, i.e. Nanophytoplankton III, appeared that was undetectable until then (Fig. 1e). It remained present throughout the duration of the experiment at rather stable concentration (< 150 cells ml^{-1}), with generally highest algal numbers for the high pCO_2 mesocosms. Nanophytoplankton IV showed similar algal concentrations, as well as having lowest abundances in the low pCO_2 addition mesocosms 2, 3 and 7 (Fig. 1f).

Figure 2 shows the phytoplankton (< 20 µm) cellular carbon (algal POC). The first maximum at $t5$ is due to the peak in nanophytoplankton around that time (Fig. 2a). Despite their relatively low numbers, their larger size results in algal POC concentrations similar to or higher than that of the more abundant (up to 70-fold higher cell abundances) but very small picoeukaryotic algae that are responsible for the second maximum of algal POC (Fig. 2b).

3.2 pCO_2-related phytoplankton trends

As expected, all mesocosms resembled each other for microbial abundances during the initial phase 0 (t – 7 to $t3$). Shortly after completing CO_2 additions (at $t7$; phase 1) the standing stock of Picophytoplankton II in the three high pCO_2 mesocosms 5, 6

BGD
9, 12309–12341, 2012

and 9 showed a negative response (Fig. 3a). This response was, however, not maintained and even reversed after nutrients were added at $t13$. It has to be noted that Picophytoplankton II was made up by 3 subpopulations that were hard to separate. A weak positive correlation with pCO_2 during phase 1, thus prior to nutrient addition, was only observed for Picophytoplankton I ($y = 16.6x + 2.0 \times 10^4$, $r^2 = 0.516$). Upon the addition of inorganic nutrients (phase 2), Picophytoplankton II became dominated by one of those subpopulations. Interestingly, the peak abundances of picophytoplankton I at $t18$ correlated strongly and positively with pCO_2 (Fig. 3b). Net growth rates increased on average from 0.15 d^{-1} at present day pCO_2 to 0.2 d^{-1} at future pCO_2. At the same time we also found positive relationships with pCO_2 for the cell abundances of Picophytoplankton II and Nanophytoplankton I (Fig. 3c and d). Nanophytoplankton III and IV furthermore showed positive correlations with pCO_2 only until 600 µatm (r^2 of 0.903 and 0.610, respectively), however, the low cell abundances (< 150 ml^{-1}) caution for over-interpretation (higher statistical error). Notwithstanding, the positive correlation between phytoplankton standing stock and pCO_2 levels at $t18$ is clearly illustrated by total algal POC (Fig. 4).

Within phase 1 of the experiment ($t4$–13), the net loss rates during the decline of the Nanophytoplankton I peak ($t6$–13) were negatively correlated with pCO_2, i.e. lower net loss rates at higher pCO_2 levels (from −0.15 d^{-1} at high pCO_2 to −0.3 d^{-1} at low pCO_2; Fig. 5a). During the decline of the Picophytoplankton II bloom ($t7$–22) the highest pCO_2 mesocosms also showed reduced net loss rates (on average -0.10 ± 0.04 d^{-1} as compared to -0.19 ± 0.03 d^{-1} for the other mesocosms; Fig. 5b). In contrast, the net loss rates after the bloom of Picophytoplankton I ($t18$–26) show a positive correlation with pCO_2 when excluding mesocosm 4 that had already declined during that period (on average -0.32 ± 0.1 d^{-1} for the mesocosms with $pCO_2 \geq 600$ µatm and -0.19 ± 0.07 d^{-1} for $pCO_2 \leq 600$ µatm; Fig. 5c). At the end of the experiment ($t27$) the Picophytoplankton I show a negative correlation with pCO_2, however, we argue below that at this stage into the experiment such a correlation is the indirect effect of viral lysis and grazing dynamics.

BGD
9, 12309–12341, 2012

3.3 Phytoplankton viruses and microzooplankton grazing

The viral community could be discriminated in 5 distinct clusters of which two (V4 and V5) are considered exclusively algal viruses (Fig. 6; Brussaard and Martínez Martínez, 2008). The abundance of viruses V4 started to increase upon the development of the Nanophytoplankton I bloom and showed its strongest increase concomitantly with the decline of this phytoplankton group (Figs. 1c and 6a). Moreover, V5 increased sharply the moment the bloom of Picophytoplankton I declined ($t18$; Figs. 1a and 6b), indicating a regulating role of viruses on the dynamics of also this phytoplankton population.

Microzooplankton grazing rates (Table 1) showed high grazing on Picophytoplankton I during the first days of the experiment (phase 0; around $0.5\,d^{-1}$). Grazing rates dropped after phase 0 down to $0.1–0.2\,d^{-1}$. No correlation with pCO_2 was observed. For unknown reasons, the dilution assay during the first half of the experiment (phase 0 and 1) did not provide good grazing data for the Picophytoplankton II. The second half of the experiment (phase 2 and 3), grazing on picophytoplankton II was substantial (on average 0.32 ± 0.21 d^{-1}) but without a trend with pCO_2. Microzooplankton grazing on Nanophytoplankton I was relatively high throughout the experiment (on average 0.51 ± 0.31 d^{-1}) with highest rates in the second half of the experiment from $t12$ (grazing between 0.6 and $1.2\,d^{-1}$).

3.4 HP dynamics

The abundances of HP in all mesocosms dropped abruptly during the first week (by 1.5×10^6 ml^{-1}; Fig. 7a), which was fully due to the decline in the high-nucleic acid (HDNA) HP population. The % HDNA-HP dropped from around 80 to 40–55 % at $t7$ (Fig. 7b). Viruses increased in abundance around 1×10^7 ml^{-1} (Fig. 8a). The concomitant decline of HP and increase in viruses resulted in a steeply increasing virus to bacterium ratio (VBR), from 25 up to 150; Fig. 8b). After $t7$ the total HP community increased steadily again (Fig. 7a). The % HDNA HP also increased again up to a maximum of 70 % at $t14$ (Fig. 7b), after which it decreased steadily resulting in an equal

BGD
9, 12309–12341, 2012

contribution of HDNA and LDNA HP towards the end of the experiment (phase 3). HP net growth rates, derived from $t5$ to the end of the experiment, correlated negatively to pCO_2, which consequently resulted in a negative correlation between HP abundance at $t28$ and pCO_2 levels (Fig. 7c). No such trend was found for virus abundances. However, the slopes of the linear regression of viruses versus HP per mesocosm plotted against pCO_2 levels resulted in a linear correlation (Fig. 8c), which suggests a stronger impact of viruses on HP dynamics at higher pCO_2.

4 Discussion

The Arctic Ocean ecosystem is particular vulnerable for OA related alterations due to the relatively high CO_2 solubility and low carbonate saturation states of its cold surface waters. Thus far, however, there is only little known about the consequences of OA on the base of the food web. In a mesocosm CO_2-enrichment experiment (overall CO_2 levels ranged from ~ 180 to 1100 µatm) in the Kongsfjord off Svalbard, we studied the consequences of OA on a natural pelagic microbial community. Overall, our results show that elevated CO_2 stimulated the growth of the smallest size range of primary producers, thereby substantially affecting the structure and functioning of the pelagic food web in the future.

4.1 Phase 0

The initial phase of the experiment showed an increase in standing stock of the phytoplankton clusters Picophytoplankton II (2–3 µm diameter) and Nanophytoplankton I (3–8 µm diameter) phytoplankton. The sum of the net growth rates of 0.5–0.55 d^{-1} with the loss rates by grazing and some viral lysis compare well with the on average 0.85 d^{-1} gross growth rate obtained by ^{13}C-uptake (De Kluijver et al., 2012). Inorganic nutrients were depleted due to the spring bloom preceding our experiment and thus, the smaller-sized phytoplankton were in competitive advantage growing on remineralised

BGD
9, 12309–12341, 2012

ammonia and inorganic phosphate (Schulz et al., 2012). Furthermore, utilization of organic nutrients and mixotrophy may also have allowed growth by these phytoplankton groups (Schulz et al., 2012). Light microscopy data showed that nano-sized (around 5 µm cell diameter, thus potentially belonging to Nanophytoplankton I) *Pseudopedinella* sp., a known mixotroph, peaked around *t*4 (A. Stuhr, personal communication, 2012). Another mixotroph Chrysophyte, i.e. *Ochromonas* sp. also developed during phase 0 and into phase 1 (A. Stuhr, personal communication, 2012). However, expressed in organic carbon, these Chrysophytes were not the dominant nanoeukayotes. Phytoplankton pigment analysis showed dominance of Prasinophyceae and Haptophyceae (Schulz et al., 2012), which are known to consist largely of pico- and nanophytoplankton, respectively. Members of the Prasinophyceae have been found to be the most abundant picophytoplankton (Zhu et al., 2005), although recently Cuvelier et al. (2010) found that picoprymnesiophytes (Haptophyceae) may also contribute to global picophytoplankton biomass. Recently, dominance of picophytoplankton has also been shown in the perennially cold ocean in the Canadian Arctic during summer (> 70 % of total cell count; Tremblay et al., 2009). Besides, some diatoms were still present but these were typically larger than detectable by the flow cytometer used in this study (Schulz et al., 2012).

We noted a clear decline in the HP standing stock during the period of CO_2 manipulations (of 0.2×10^5 HP ml^{-1} d^{-1}), matching the decline in HP production (Motegi et al., 2012) and most likely due to viral lysis. Virus-mediated mortality rates were high (on average 3.9-fold higher than throughout the rest of the experiment, i.e. 90 % d^{-1} versus 23 % d^{-1}), whereas grazing by heterotrophic nanoflagellates accounted at maximum for one third of the HP mortality (W. Weinbauer, personal communication, 2012). The estimated burst size was on average 7 viruses per lysed bacterium cell (estimated from the net loss of HP and net production of viruses), which seems somewhat low (see review by Parada et al., 2006) although Middelboe and colleagues (2002) have observed such low burst sizes in Arctic water during summer. Interestingly, specifically the HDNA-HP were affected. Phage proliferation has been found to depend on host metabolism

BGD
9, 12309–12341, 2012

(c.q. HP host generation times; see review by Weinbauer, 2004) and HDNA-HP have been reported to represent the metabolic active members of the microbial community (Lebaron et al., 2001). However, some contrasting studies did show that LDNA-HP can also be an active part of the microbial population (Zubkov et al., 2001; Brussaard et al., 2005; Wang et al., 2009). Preferential grazing on HDNA HP has been implied (Gasol et al., 1999; Vaque, 2001), although cell size instead of metabolic activity might have been the underlying reason. Still, the selective loss of HDNA-HP due to viral lysis has been, to our knowledge, not yet reported.

4.2 Phase 1

This phase is the only period in which the sole effect of the CO_2 treatment could be determined as nutrients were not added yet ($t13$). Phase I was dominated in algal POC by nanophytoplankton, peaking around $t5$. The study by Schulz et al. (2012) showed that the Haptophyceae was the principal algal class. Although no obvious correlation between the peak abundances and pCO_2 was recorded, we did find a negative correlation of the net loss rates (obtained from the decline in net abundances) with pCO_2. Highest net loss rates were observed for the low CO_2 mesocosms (~ 180–270 µatm); 0.30 d^{-1} as compared to 0.15 d^{-1} for the future CO_2 mesocosm, which corresponded to the higher microzooplankton grazing rate at the low CO_2 level as compared to the rate at high pCO_2 at $t7$. OA has been reported not to affect microzooplankton abundance or grazing activity (Suffrian et al., 2008), however in contrast to our study, neither phytoplankton composition nor succession differed between their CO_2 treatments (Riebesell et al., 2007). Although grazing rates matched the net loss rates, viral lysis also accounted for half the losses, which implies that the nanophytoplankton still grew but that the higher loss rates resulted in the decline of the algal bloom. De De Kluijver and coworkers (2012) indeed still recorded ^{13}C-utilization by the nanophytoplankton during $t5$ to $t10$.

With half the net decline in Nanophytoplankton I abundance to be due to viral lysis, we found viral burst sizes (i.e. the number of newly produced viruses released per

BGD
9, 12309–12341, 2012

lysing host cell) of 540–764 for the different mesocosms. The literature shows comparable burst sizes for nanophytoplankton host-virus model systems from the Haptophyceae class, e.g. 350–600 for *Phaeocystis globosa* and *P. pouchetii*, 400–1000 for *Emiliania huxleyi* (see review by Brussaard and Martínez Martínez, 2008).

The utilization of the organic matter released by viral lysis of the HP (phase 0) and the nanophytoplankton (phase 1) resulted in a steady increase in HP abundance after *t*5. Based on half of the nanophytoplankton lost due to viral lysis, a HP carbon conversion of 12 fg C cell^{-1} (Fukuda et al., 1998), a HP growth efficiency of 30 % (Motegi et al., 2012) and taking a 50 % mortality of the heterotrophic HP into account (Motegi et al., 2012), we estimated that the cellular carbon released by viral lysis (about 30 µg C l^{-1}) sustained about a third of the gross HP carbon demand during phase 2. Extracellular enzyme activities and bacterial protein production indeed increased already during phase 0 and peaked during *t*5 to *t*10 (Piontek et al., 2012), concomitantly with the virally-induced decline in Nanophytoplankton I.

The abundance of Picophytoplankton II peaked at *t*7 but showed 2-fold lower densities for the high CO_2 mesocosms (~ 650–1100 µatm). It is unclear whether these algae became negatively affected in their growth at the higher future CO_2 levels or the loss rates for the high pCO_2 mesocosms were enhanced (grazing estimates on Picophytoplankton II during this phase failed for the low pCO_2 mesocosm). Hopkins et al. (2010) reported a similar finding for a mesocosm experiment in a fjord in Norway, showing lower abundances of large picophytoplankton under high pCO_2 (750 µatm) than in the present day CO_2 enclosure. Still, Picophytoplankton II formed a complex cluster with 2–3 subpopulations that could not be separated from each other. A shift to one subpopulation in response to elevated pCO_2 may also have been responsible for the obtained results.

During phase 1 the abundances of the small-sized Picophytoplankton I (average 1.2 µm cell diameter) increased steadily. The average net growth rates of the Picophytoplankton I in this phase were 0.14 ± 0.03, 0.15 ± 0.03 and 0.17 ± 0.02 d^{-1} for the low, intermediate and high pCO_2 mesocosms. Correcting for grazing loss, the gross growth

BGD
9, 12309–12341, 2012

rates were overall 0.1 d^{-1} higher. Already prior to nutrient addition, a weak positive correlation between abundance and pCO_2 emerged, suggesting that elevated CO_2 stimulated the growth of these very small sized phytoplankton (0.8–2 µm). The trend developed strongly into phase 2 (see Sect. 4.3), emphasizing that elevated CO_2 stimulates growth and nutrient utilization (Schulz et al., 2012) leading to enhanced production of the smallest size range of primary producers.

4.3 Phase 2

Phase 2 represents the initial period upon the addition of inorganic nutrients, allowing for potential growth of larger sized phytoplankton. Elevated CO_2 in combination with nutrient addition stimulated the growth of the smaller-sized phytoplankton as shown by the positive correlation of algal POC at $t18$ with pCO_2. These results were supported by the higher uptake rates of the added inorganic nutrients for the highest pCO_2 mesocosms (Schulz et al., 2012). Interestingly, the prevailing group of algae during this period was still the picophytoplankton (particularly cluster I) and to a lesser extent the nanophytoplankton. Algal pigment analysis and light microscopic screening indicated that Prasinophyceae was the dominant algal class and larger sized phytoplankton like diatoms were largely absent still (Schulz et al., 2012).

Our results clearly show that the very small-sized picophytoplankton became dominant under increased CO_2 levels, indicating that this group does not or still inefficiently apply carbon concentrating mechanisms (CCMs). Diffusion of CO_2 is typically not expected to limit photosynthesis in the very small-sized phytoplankton (Giordano et al., 2005), although CCMs were identified for the picophytoplankter *Micromonas pusilla* (Worden et al., 2009). Yet, despite their small size (and thus large surface to volume ratio) their diffusive CO_2 uptake seems insufficient and their CO_2 sensitive photosynthesis benefitted from elevated pCO_2. Only a small response to OA (e.g. 10 %, The Royal Society, 2005 and references therein) can still result in dominance over time under the assumptions that the loss factors (grazing, viral lysis) do not show direct

BGD
9, 12309–12341, 2012

responses to elevated pCO_2 and other growth variables are not limiting the growth. We found no evidence that grazing or viral lysis rates were directly affected by elevated CO_2 levels and nutrients and irradiance were non-limiting at the time. The higher abundances of Picophytoplankton I at high pCO_2 resulted thus from somewhat enhanced growth rates. Paulino et al. (2008) reported an increased abundance of picophytoplankton in a high CO_2 mesocosm, however, this was towards the end of the experiment when all nutrients were depleted. During another Norwegian fjord mesocosm experiment, still nutrient-replete, the total number of small-sized picophytoplankton did not change under increased pCO_2 (750 µatm; Hopkins et al., 2010; Newbold et al., 2012). The abundances based on quantitative PCR of specifically the picophytoplankter *Micromonas pusilla*, nevertheless, enhanced significantly (Meakin and Wyman, 2011). A similar trend was observed a few years earlier at the same location, time of the year and experimental set-up, this time based on a *M. pusilla*-like flow cytometric signature (Engel et al., 2008). Meakin and Wyman (2011) showed that the picophytoplankter Bathycoccus (also belonging to the Prasinophyceae) was not affected by the increased CO_2 concentrations. Although we have no knowledge of the actual species that are represented by our flow cytometric clusters, our data show (1) the dominance of the picoeukaryotic phytoplankton in polar waters and (2) the potential ecological importance this group will have in future oceans.

High grazing pressure kept the abundances of Nanophytoplankton I under control during phase 2 (on average $0.74 \pm 0.31\ d^{-1}$). Our data suggest that grazing was not affected by pCO_2 (a relationship with pCO_2 could not be tested for shortage of grazing rates in the high CO_2-mesocosms) and viral lysis was not an substantial loss factor at the time, implying that the higher standing stock of the Nanophytoplankton I under elevated CO_2 was also due to higher growth rates (as for the Picophytoplankton I).

For the Picoeukayotes I viral lysis was the dominant loss factor, with the steepest increase of virus population V observed for the highest pCO_2 mesocosms (in agreement with the strongest decline of Picophytoplankton I at these CO_2 levels). Estimated burst sizes ranged between 119 and 245, matching the published values for Prasinophyte

BGD
9, 12309–12341, 2012

picophytopankton host-virus model systems (e.g. 72–360 for *Micromonas pusilla*; Waters and Chan, 1982; Baudoux et al., 2008). The resultant release of cellular organic carbon due to viral lysis of the Picophytoplankton I increased with CO_2 level, i.e. 7, 10 and 20 µg C l^{-1} for the low, intermediate and high pCO_2 mesocosms. Based on the HP net growth rate of 0.2×10^5 cells ml^{-1} d^{-1}, a BGE of 30 % and low mortality (Mortegi et al., 2012), viral lysis accounted for 15 to 42 % of the gross HP C-demand.

4.4 Phase 3

Despite the enhanced release of the lysing algal cells in the highest pCO_2 mesocosms that continued into phase 3, the HP standing stock was lower at elevated CO_2. This may have been due to increased heterotrophic nanoflagellate grazing rates (W. Weinbauer, personal communication, 2012), but potentially higher viral lysis rates due to higher VBR and therefore encounter rate may have been an additional reason.

During this last phase of the experiment picophytoplankton were still most abundant but the biomass share of the nanophytoplankton became more important, equaling picophytoplankton. Schulz et al. (2012) showed that the Haptophycease, containing many nanoeukaryotic phytoplankton species, increased in abundance during this phase. The same authors showed, furthermore, that larger-sized photoautotrophs such as the Dinophyceae became an important group and were positively correlated to elevated CO_2. In contrast, the growth of diatoms and Chlorophyceae was reduced at elevated CO_2, most likely due to diminished nutrient availability (inorganic nutrients became depleted during the second half of phase 3). Species in these phytoplankton classes often have efficient CCMs that allow for optimal photosynthesis and growth at ambient (and past) CO_2 concentrations and, therefore, are not (or only minimally) affected by increased CO_2 levels (Giordano et al., 2005; Engel et al., 2008; Rost et al., 2008).

BGD
9, 12309–12341, 2012

5 Conclusions

The most prominent finding of our study is the profound effect of OA on the composition and growth of the Arctic phytoplankton community, i.e. the picoeukaryotic photoautotrophs and to a lesser extent the nanophytoplankton prospered. This mesocosm experiment took into account at least 4 of the 7 future research recommendation stated by Rost et al. (2008), namely it mimicked the environmental conditions as closely as possible, was community based (microbial food web), involved the interactive effects of multiple environmental variables in combination with CO_2, and tried to unravel the underlying mechanisms for the observed responses by taking into account loss factors such as grazing and viral lysis. These aspects in combination with our focus on the smaller-sized phytoplankton contributed largely to a more detailed and inclusive understanding of ecological responses to changes in CO_2.

A shift towards the smallest phytoplankton as a result of OA will have direct consequences for the structure and functioning of the pelagic food web and thus for the biogeochemical cycles. Further trophic levels will reduce the transfer of matter and energy to higher predators, and the importance of the microbial food web will increase. The dominant pico- and nanophytoplankton groups were found prone to viral lysis, thereby shunting the carbon that enters the biological pool via photosynthesis, from carbon accumulation in living organisms into the dissolved pools of organic carbon (Suttle, 2007). Microbial communities incorporate these pools, thereby converting much of it to CO_2 again by respiration and subsequently influencing the efficiency of the biological pump (Brussaard et al., 2008).

The here discussed ecological changes by OA do not stand alone as global climate change impacts the polar waters also through temperature rise, shift in wind, precipitation and circulation (Schofield et al., 2010). Phytoplankton growth-relevant factors such as light, pCO_2, temperature, nutrient availability and salinity are all under change due to global warming. The increment in surface water temperature will reduce the solubility of CO_2 in the Arctic seawater, and the mean cell size of phytoplankton community

BGD
9, 12309–12341, 2012

(Daufresne et al., 2009). Moreover, increased surface water temperature and glacier and sea-ice melt will strengthen vertical stratification, which in the Canadian Arctic waters has been reported to stimulate picophytoplankton and reduce nanophytoplankton abundance (Li et al., 2009). Thus, in the global climate-driven changing Arctic Ocean the smallest phytoplankton are expected to flourish as a general result of OA that is further reinforced in summer by increased temperature-imposed vertical stratification.

Acknowledgements. This work is a contribution to the "European Project on Ocean Acidification" (EPOCA) which received funding from the European Community's Seventh Framework Programme (FP7/2007–2013) under grant agreement no. 211384. The research leading to these results has also received funding from the European Union Seventh Framework Program (FP7/2007-2-13) under grant agreement no. 228224, MESOAQUA. We gratefully acknowledge the logistical support of Greenpeace International for its assistance with the transport of the mesocosm facility from Kiel to Ny-Ålesund and back to Kiel. We also thank the captains and crews of M/V *ESPERANZA* of Greenpeace and R/V *Viking Explorer* of the University Centre in Svalbard (UNIS) for assistance during mesocosm transport and during deployment and recovery in Kongsfjorden. We thank the staff of the French-German Arctic Research Base at Ny-Ålesund (AWIPEV), in particular Marcus Schumacher, for on-site logistical support. We are indebted to Richard Bellerby for providing DIC data, Sebastian Krug for general support and Jan Czerny for his advice on the sampling of the mesocosms for phytoplankton losses. We finally thank Maarten van Loon for arranging accommodation at the Dutch Station.

References

Baudoux, A.-C. and Brussaard, C. P. D.: Influence of irradiance on viral-algal host interactions, J. Phycol., 44, 902–908, 2008.

Bellerby, R. G. J., Silyakova, A., Nondal, G., Slagstad, D., Czerny, J., De Lange, T., and Ludvig, A.: Marine carbonate system evolution during the EPOCA Arctic pelagic ecosystem experiment in the context of simulated future Arctic ocean acidification, Biogeosciences, accepted, 2012.

Boyd, P. W. and Doney, S. C.: Modelling regional responses by marine pelagic ecosystems to global climate change, Geophys. Res. Lett., 29, 1806, doi:10.1029/2001GL014130, 2002.

BGD

9, 12309–12341, 2012

Brussaard, C. P. D.: Optimization of procedures for counting viruses by flow cytometry, Appl. Environ. Microbiol., 70, 1506–1513, 2004.
Brussaard, C. P. D. and Martínez Martínez, J.: Algal bloom viruses, Plant Viruses 2, 1–13, 2008.
Brussaard, C. P. D., Gast, G. J., Van Duyl, F. C., and Riegman, R.: Impact of phytoplankton bloom magnitude on pelagic microbial food web, Mar. Ecol. Progr. Ser., 144, 211–221, 1996.
Brussaard, C. P. D., Mari, X., Van Bleijswijk, J. D. L. and Veldhuis, M. J. W.: A mesocosm study of *Phaeocystis globosa* population dynamics, II. Significance for the microbial community, Harmful Algae, 4, 875–893, 2005.
Brussaard, C. P. D., Wilhelm, S. W, Thingstad, F., Weinbauer, M. G., Bratbak, G., Heldal, M., Kimmance, S. A., Middelboe, M., Nagasaki, K., Paul, J. H., Schroeder, D. C., Suttle, C. A., Vaqué, D., and Wommack, K. E.: Global-scale processes with a nanoscale drive: the role of marine viruses, ISME J., 2, 575–578, 2008.
Cuvelier, M. J., Allenc, A. E., Monier, A., McCrow, J. P., Messié, M., Tringe, S. G., Woyke, T., Welsh, R. M., Ishoey, T., Lee, J., Binder, B. J., DuPont, C. L., Latasa, M., Guigand, C., Buck. K. R., Hilton, J., Thiagarajan, M., Caler, E., Read, B., Lasken, R. S., Chavez, F. P., and Worden, A. Z.: Targeted metagenomics and ecology of globally important uncultured eukaryotic phytoplankton, P. Natl. Acad. Sci. USA, 107, 14679–14684, 2010.
Daufresne, M., Lengfellner, K., and Sommer, U.: Global warming benefits the small in aquatic ecosystems, P. Natl. Acad. Sci. USA, 106, 12788–12793, 2009.
de Kluijver, A., Soetaert, K., Czerny, J., Schulz, K. G., Boxhammer, T., Riebesell, U., and Middelburg, J. J.: A ^{13}C labelling study on carbon fluxes in Arctic plankton communities under elevated CO_2 levels, Biogeosciences Discuss., 9, 8571–8610, doi:10.5194/bgd-9-8571-2012, 2012.
Engel, A., Schulz, K. G., Riebesell, U., Bellerby, R., Delille, B., and Schartau, M.: Effects of CO_2 on particle size distribution and phytoplankton abundance during a mesocosm bloom experiment (PeECE II), Biogeosciences, 5, 509–521, doi:10.5194/bg-5-509-2008, 2008.
Falkowski, P. G.: The microbial engines that drive Earth's biogeochemical cycles, Science, 320, 1034–1039, 2008.
Feng, Y., Hare, C. E., Leblanc, K., Rose, J. M., Zhang, Y., DiTullio, G. R., Lee, P. A., Wilhelm, S. W., Rowe, J. M, Sun, J., Nemcek, N., Gueguen, C., Passow, U., Benner, I., Brown, C., and Hutchins, D. A.: Effects of increased pCO_2 and temperature on the North Atlantic spring

BGD
9, 12309–12341, 2012

bloom, I. The phytoplankton community and biogeochemical response, Mar. Ecol. Prog. Ser., 388, 13–25, 2009.
Fukuda, R., Ogawa, H., Nagata, T., and Koike, I.: Direct determination of carbon and nitrogen contents of natural bacterial assemblages in marine environments, Appl. Enivon. Microbiol., 64, 3352–3358, 1998.
Gasol, J. M., Zweifel, U. L., Peters, F., Fuhrman, J. A., and Hagström, Å.: Significance of size and nucleic acid content heterogeneity as measured by flow cytometry in natural planktonic bacteria, Appl. Environ. Microbiol., 65, 4475–4483, 1999.
Giordano, M., Beardall, J., and Raven, J. A.: CO_2 concentrating mechanisms in algae: mechanisms, environmental modulation, and evolution, Annu. Rev. Plant Biol., 56, 99–131, 2005.
Hoegh-Guldberg, O. and Bruno, J. F.: The Impact of Climate Change on the World's Marine Ecosystems, Science, 328, 1523–1528, 2010.
Hopkins, F. E., Turner, S. M., Nightingale, P. D., Steinke M., Bakker, D., and Liss, P. S.: Ocean acidification and marine trace gas emissions, P. Natl. Acad. Sci. USA, 107, 760–765, 2010.
Landry, M. R. and Hassett, R. P.: Estimating the grazing impact of marine micrzooplankton, Mar. Biol., 67, 283–288, 1982.
Lebaron, P., Servais, P., Agogué, H., Courties, C., and Joux, F.: Does the high nucleic acid content of individual bacterial cells allow us to discriminate between active cells and inactive cells in aquatic systems?, Appl. Environ. Microbiol., 67, 1775–1782, 2001.
Li, W. K. W., McLaughlin, F. A., Lovejoy, C., and Carmack, E. C.: Smallest algae thrive as the Arctic Ocean freshens, Science, 326, 539 pp., 2009.
Marie, D., Brussaard, C. P. D., Partensky, F., and Vaulot, D.: Enumeration of phytoplankton, bacteria and viruses in marine samples, in: Current protocols in cytometry, edited by: Robinson, J. P., Darzynkiewicz, Z., Dean, P. N., Orfao, A., Rabinovitch, P. S., Stewart, C. C., Tanke, H. J., and Wheeless, L. L., John Wiley and Sons, 11.11.11–11.11.15, 1999.
Meakin, N. G. and Wyman, M.: Rapid shifts in picoeukaryote community structure in response to ocean acidification, ISME J., 5, 1397–1405, 2011.
Middelboe, M., Nielsen, T. G., and Bjørnsen, P. K.: Viral and bacterial production in the North Water: in situ measurements, batch-culture experiments and characterization and distribution of a virus-host system, Deep-Sea Res. Pt. II, 49, 5063–5079, 2002.
Motegi, C., Tanaka, T., Piontek, J, Brussaard, C. P. D., Gattuso, J. P., and Weinbauer, M. G.: Effect of CO_2 enrichment on bacterial production and respiration and on bacterial carbon metabolism in Arctic waters, Biogeosciences, accepted, 2012.

BGD
9, 12309–12341, 2012

Newbold, L. K., Oliver, A. E., Booth, T., Tiwari, B., DeSantis, T., Maguire, M., Andersen, G., Van der Gast, C. J., and Whiteley, A. S.: The response of marine picoplankton to ocean acidification, Environ. Microbiol., 14, 2293–2307, doi:10.1111/j.1462-2920.2012.02762.x, 2012.

Parada, V., Herndl, G. J., and Weinbauer, M. G.: Viral burst size of heterotrophic prokaryotes in aquatic systems, J. Mar. Biol. Assoc. UK, 86, 613–621, 2006.

Paulino, A. I., Egge, J. K., and Larsen, A.: Effects of increased atmospheric CO_2 on small and intermediate sized osmotrophs during a nutrient induced phytoplankton bloom, Biogeosciences, 5, 739–748, doi:10.5194/bg-5-739-2008, 2008.

Piontek, J., Borchard, C., Sperling, M., Schulz, K. G., Riebesell, U., and Engel, A.: Response of bacterioplankton activity in an Arctic fjord system to elevated pCO_2: results from a mesocosm perturbation study, Biogeosciences Discuss., 9, 10467–10511, doi:10.5194/bgd-9-10467-2012, 2012.

Riebesell, U. and Tortell, P. D.: Effects of ocean acidification on pelagic organisms and ecosystems, in: Ocean Acidification, Oxford University Press, Oxford, UK, 99–121, 2011.

Riebesell, U., Schulz1, K. G., Bellerby, R. G. J., Botros, M., Fritsche, P., Meyerhofer, M., Neill, C., Nondal, G., Oschlies, A., Wohlers, J., and Zollner, E.: Enhanced biological carbon consumption in a high CO_2 ocean, Nature, 450, 545–549, 2007.

Riebesell, U., Czerny, J., von Bröckel, K., Boxhammer, T., Büdenbender, J., Deckelnick, M., Fischer, M., Hoffmann, D., Krug, S. A., Lentz, U., Ludwig, A., Muche, R., and Schulz, K. G.: Technical Note: A mobile sea-going mesocosm system: New opportunities for ocean change research, Biogeosciences, in press, 2012.

Rose, J. M., Feng, Y., Gobler, C. J., Gutierrez, R., Hare, C. E., Leblanc, K., and Hutchins, D. A.: Effects of increased pCO_2 and temperature on the North Atlantic spring bloom, II. Microzooplankton abundance and grazing, Mar. Ecol. Prog. Ser., 388, 27–40, 2009.

Rost, B., Zondervan, I., and Wolf-Gladrow, D.: Sensitivity of phytoplankton to future changes in ocean carbonate chemistry: current knowledge, contradictions and research directions, Mar. Ecol. Prog. Ser., 373, 227–237, 2008.

Ruardij, P., Veldhuis, M. J. W., and Brussaard, C. P. D.: Modelling the development and termination of a *Phaeocystis* bloom, Harmful Algae, 4, 941–963, 2005.

Schofield, O., Ducklow, H. W., Martinson, D. G., Meredith, M. P., Moline, M. A., and Fraser, W. R.: How Do Polar Marine Ecosystems Respond to Rapid Climate Change?, Science, 328, 1520–1523, 2010.

BGD
9, 12309–12341, 2012

Schulz, K. G., Bellerby, R. G. J., Brussaard, C. P. D., Büdenbender, J., Czerny, J., Engel, A., Fischer, M., Koch.Klavsen, S., Krug, S., Lischka, S., Ludwig, A., Meyerhöfer, M., Nondal, G., Silyakova, A., Stuhr, A., and Riebesell, U.: Temporal biomass dynamics of an Arctic plankton bloom in response to increasing levels of atmospheric carbon dioxide, Biogeosciences, in press, 2012.

Suffrian, K., Simonelli, P., Nejstgaard, J. C., Putzeys, S., Carotenuto, Y., and Antia, A. N.: Microzooplankton grazing and phytoplankton growth in marine mesocosms with increased CO_2 levels, Biogeosciences, 5, 1145–1156, doi:10.5194/bg-5-1145-2008, 2008.

Suttle, C. A.: Marine viruses – major players in the global ecosystem, Nat. Rev. Microbiol., 5, 801–812, 2007.

The Royal Society: Ocean acidification due to increasing atmospheric carbon dioxide, Policy Document 12/05, Roy. Soc. Rep., Royal Society, London, 12, 2005.

Tortell, P. D., DiTullio, G. R., Sigman, D. M., and Morel, F. M. M.: CO_2 effects on taxonomic composition and nutrient utilization in an Equatorial Pacific phytoplankton assemblage, Mar Ecol. Prog. Ser., 23, 37–43, 2002.

Tremblay, G., Belzile, C., Gosselin, M., Poulin, M., Roy, S., and Tremblay, J.-E.: Late summer phytoplankton distribution along a 3500 km transect in Canadian Arctic waters: strong numerical dominance by picoeukaryotes, Aquat. Micr. Ecol., 54, 55–70, 2009.

Vaqué, D., Casamayor, E. O., and Gasol, J. M.: Dynamics of whole community bacterial production and grazing losses in seawater incubations as related to the changes in the proportions of bacteria wit different DNA content, Aquat. Microb. Ecol., 25, 163–177, 2001.

Veldhuis, M. J. W. and Kraay, G. W.: Phytoplankton in the subtropical Atlantic Ocean: Towards a better assessment of biomass and composition, Deep-Sea Res., 51, 507–530, 2004.

Wang, Y., Hammes, F., Boon, N., Chami, M., and Egli, T.: Isolation and characterization of low nucleic acid (LNA)-content bacteria, ISME J., 3, 889–902, 2009.

Waters, R. E. and Chan, A. T.: *Micromonas pusilla* virus: the virus growth cycle and associated physiological events within thehost cells; host range mutation, J. Gen. Virol., 63, 199–206, 1982.

Weinbauer, M. G.: Ecology of prokaryotic viruses, FEMS Microbiol. Rev., 28, 127–181, 2004.

Worden, A. Z., Lee, J.-H., Mock, T., Rouzé, P., Simmons, M. P., Aerts, A. L., Allen, A. E., Cuvelier, M. L., Derelle, E., Everett, M. V., Foulon, E., Grimwood, J., Gundlach, H., Henrissat,H., Napoli, C., McDonald, S. M., Parker, M. S., Rombauts, S., Salamov, A., Von Dassow, P., Badger, J. H., Coutinho, P. M., Demir, E., Dubchak, I., Gentemann, C., Eikrem, W., Gready, J. E.,

BGD
9, 12309–12341, 2012

John, U., Lanier, W., Lindquist, E. A., Lucas, S., Mayer, K. F. X., Moreau, H., Not, F., Otillar, R., Panaud, O., Pangilinan, J., Paulsen, I., Piegu, B., Poliakov, A., Robbens, S., Schmutz, J., Toulza, E., Wyss, T., Zelensky, A., Zhou, K., Armbrust, E. V., Bhattacharya, D., Goodenough, U. W., Van de Peer, Y., and Grigoriev, I. V.: Green Evolution and Dynamic Adaptations Revealed by Genomes of the Marine Picoeukaryotes *Micromonas*, Science, 324, 268–272, 2009.

Zhu, F., Massana, R., Not, F., Marie, D., and Vaulot, D.: Mapping of picoeucaryotes in marine ecosystems with quantitative PCR of the 18S rRNA gene, FEMS Microbiol. Ecol., 52, 79–92, 2005.

Zubkov, M. V., Fuchs, B. M., Burkhill, P. H., and Amann, R.: Comparison of Cellular and Biomass Specific Activities of Dominant Bacterioplankton Groups in Stratified Waters of the Celtic Sea, Appl. Environ. Microbiol., 67, 5210–5218, 2001.

BGD
9, 12309–12341, 2012

Table 1. Microzooplankton grazing rates on phytoplankton (d^{-1}) for 3 mesocosms representing low, intermediate (mid) and high pCO_2 levels. Mesocosm M3 (low, i.e. present time pCO_2) was sampled as reference to mesocosm M5 and M8. Failed assays for specific phytoplankton clusters are indicated by –.

Mesocosms (pCO_2)	Picophytoplankton I			Picophytoplankton II			Nanophytoplankton I		
Day	3 (low)	8 (mid)	5 (high)	3 (low)	8 (mid)	5 (high)	3 (low)	8 (mid)	5 (high)
1	0.54	0.35		–	–		0.29	0.11	
3	0.51			–			0.04		
7	0.07		0	–		0.09	0.34		0.15
12	–	0.09		–	0.01		0.66	0.52	
16	0.10	0.07		–	–		1.24	0.57	
20	0.08			0.39			0.98		
22	–	0.12		0	0.76		0.83	0.77	
24	0		0.16	0.11		0.38	0,72		0.32
26	0.18	0.09		0.35	0.35		0.65	0.65	
28	0		0.17	0.29		0.27	0.31		0.53

BGD
9, 12309–12341, 2012

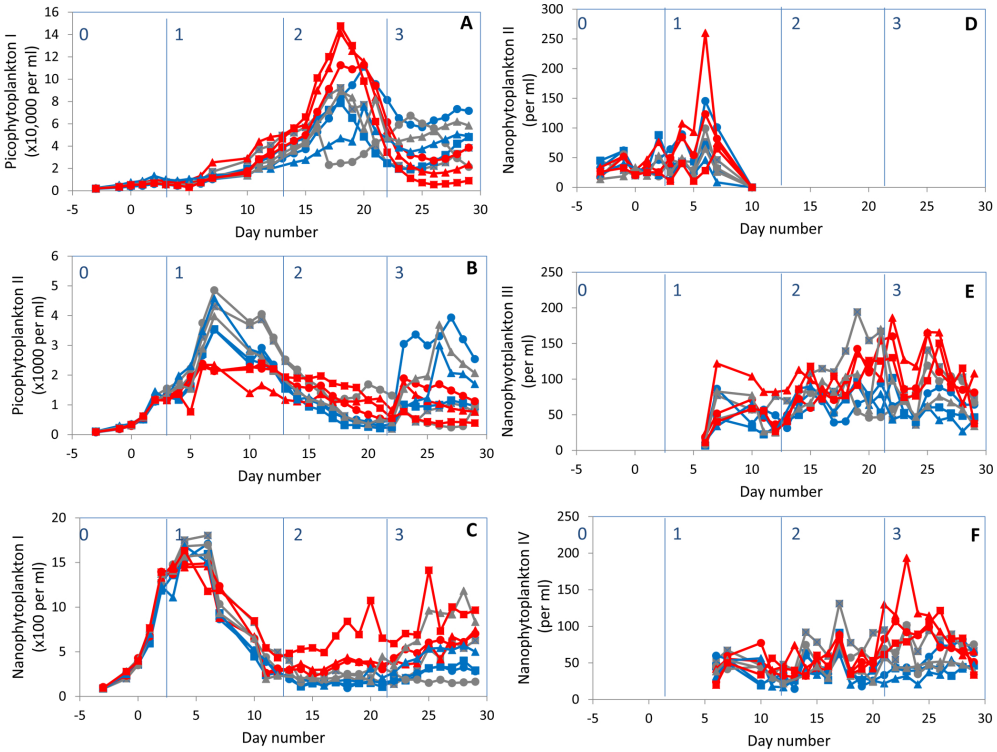

Fig. 1. Temporal dynamics of depth-integrated (0.3–12 m) picophytoplankton cluster I **(A)**, picophytoplankton cluster II **(B)**, Nanophytoplankton I **(C)**, Nanophytoplankton II **(D)**, Nanophytoplankton III **(E)** and Nanophytoplankton IV **(F)**. Only eukaryotic photosynthetic organisms were detected. Low CO_2 treatments are blue, intermediate CO_2 treatments grey and high CO_2 treatments are red colored. In order of low, intermediate and high pCO_2 mesocosms, the circles represent mesocosms M3, M4 and M6; triangles M7, M8 and M5; and squares M2, M1 and M9, respectively.

BGD
9, 12309–12341, 2012

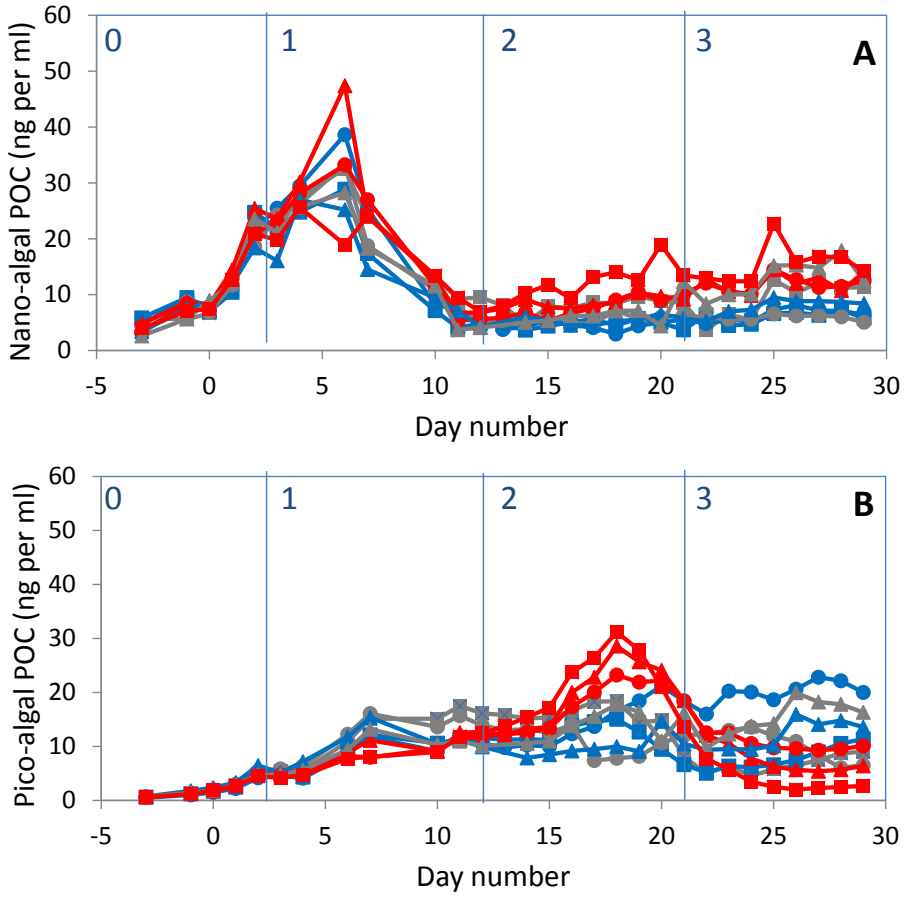

Fig. 2. Temporal development of algal particular organic carbon (POC) for total picophytoplankton **(A)** and nanophytoplankton **(B)**. For color and symbol coding see Fig. 1.

BGD
9, 12309–12341, 2012

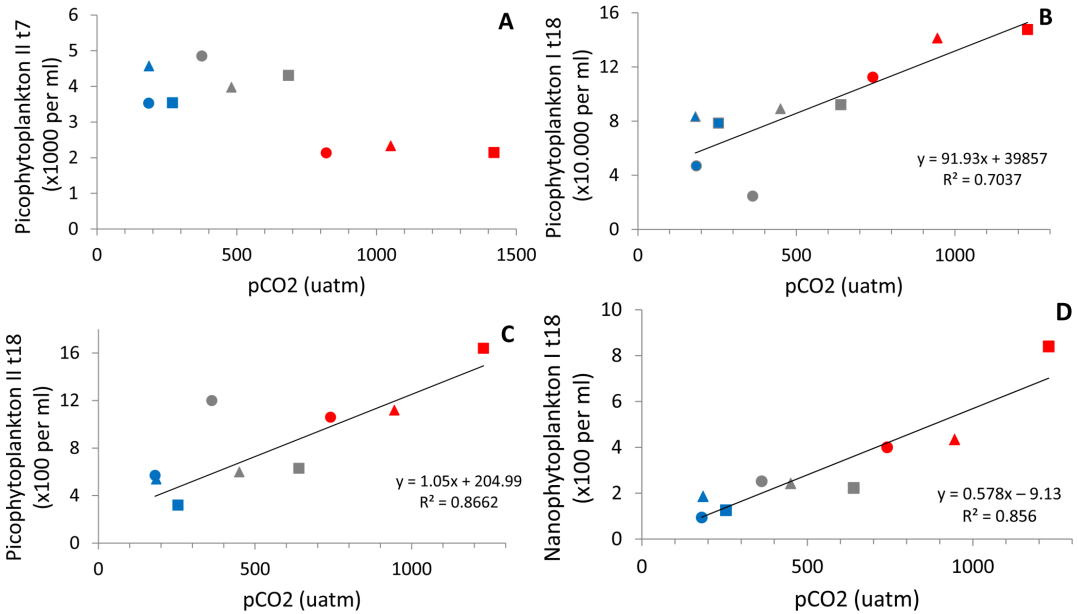

Fig. 3. Phytoplankton cell abundance versus actual pCO_2 for Picophytoplankton II on $t7$ **(A)**, Picophytoplankton I on $t18$ **(B)**, Picophytoplankton II on $t18$ **(C)**, and Nanophytoplankton I on $t18$ **(D)**. For **(B–D)** the CO_2 concentrations plotted were the averages of $t8$–$t18$. For color and symbol coding see Fig. 1.

BGD
9, 12309–12341, 2012

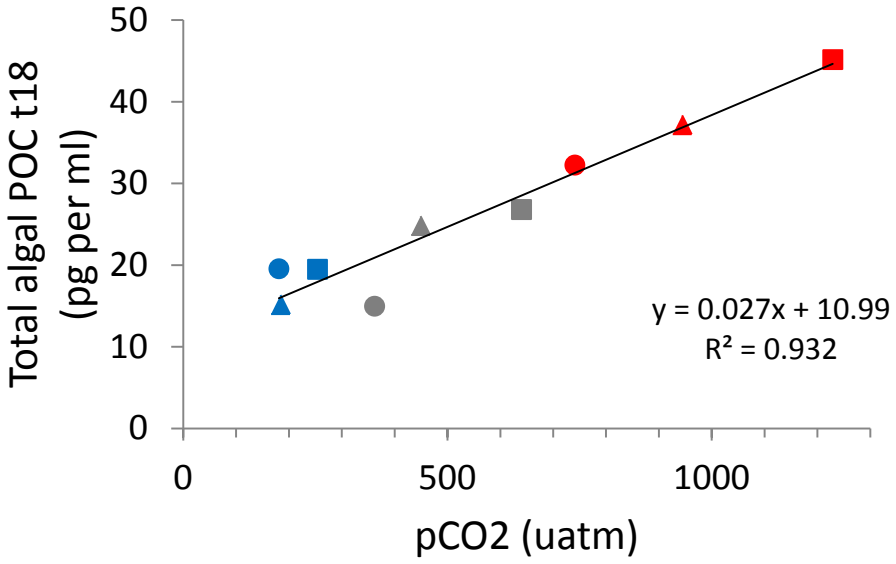

Fig. 4. Total algal POC versus pCO_2. The CO_2 concentrations plotted were the averages of $t8$–$t18$. For color and symbol coding see Fig. 1.

BGD
9, 12309–12341, 2012

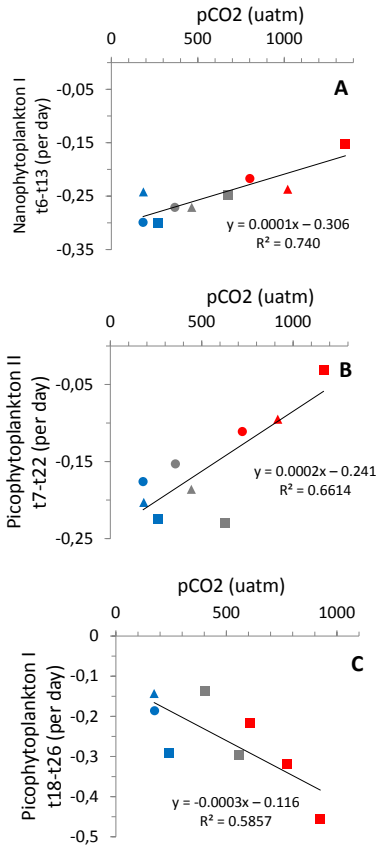

Fig. 5. Specific growth rates determined from the net phytoplankton abundances versus pCO_2. Nanophytoplankton I from *t*6–*t*13 **(A)**, Picophytoplankton II from *t*7–*t*22 **(B)**, and Picophytoplankton I from *t*18–*t*26 **(C)**. A negative growth rate indicates cell loss. The CO_2 concentrations plotted were the averages for the specific time periods indicated. For color and symbol coding see Fig. 1.

BGD
9, 12309–12341, 2012

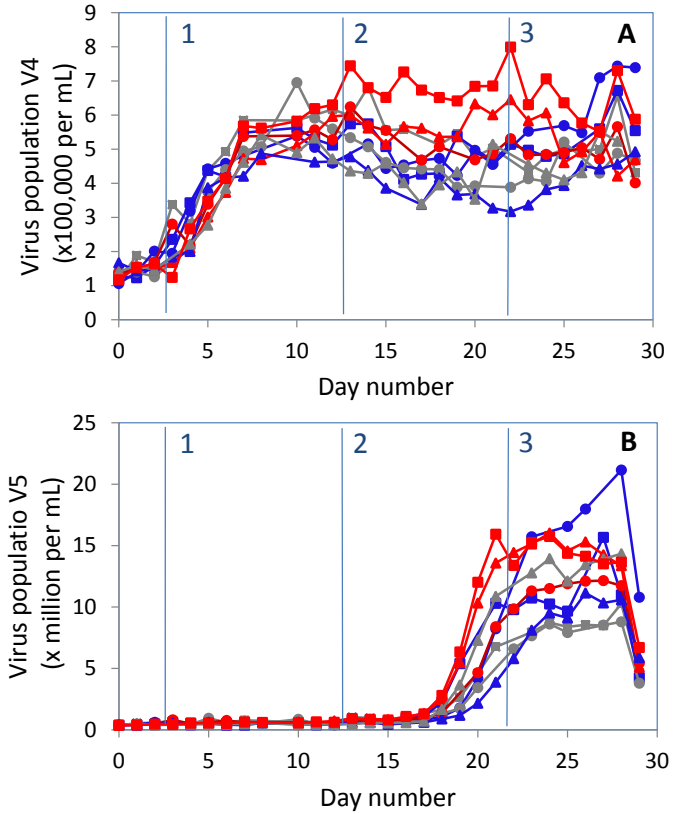

Fig. 6. Temporal dynamics of virus cluster V4, indicative for larger algal viruses infecting Nanophytoplankton I **(A)**, and V5, most likely infecting Picoplankton I **(B)**. For color and symbol coding see Fig. 1.

BGD
9, 12309–12341, 2012

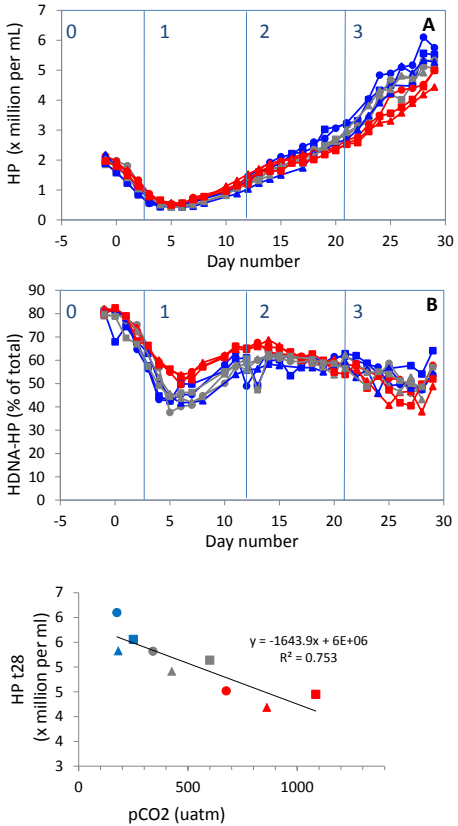

Fig. 7. Temporal development of heterotrophic prokaryotes HP **(A)**, HDNA-HP **(B)**. The abundance of HP at *t*28 plotted versus pCO_2 (average of *t*8–*t*27) is plotted in **(C)**. For color and symbol coding see Fig. 1.

BGD
9, 12309–12341, 2012

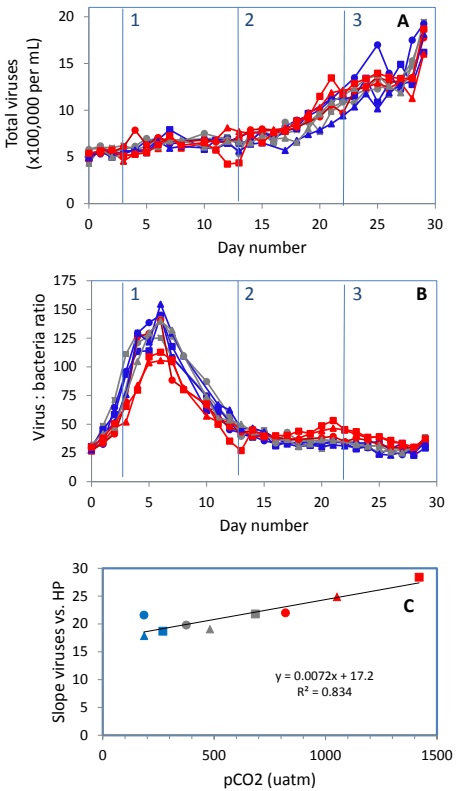

Fig. 8. Temporal dynamics of total viruses **(A)** and the virus to HP ratio **(B)**. Furthermore, the slope of viruses versus HP, thus representing the average number of viruses per HP, for each mesocosm plotted versus the concurrent pCO_2 (averaged over *t*8–*t*27) in **(C)**. For color and symbol coding see Fig. 1.

BGD
9, 12309–12341, 2012